Self-energy in surface electron spectroscopy: II. Surface excitation on real metal surfaces

1998 J. Phys.: Condens. Matter 10 1753

(http://iopscience.iop.org/0953-8984/10/8/010)

J. Phys.: Condens. Matter **10** (1998) 1753–1765. Printed in the UK PII: S0953-8984(98)87359-1

Self-energy in surface electron spectroscopy: II. Surface excitation on real metal surfaces

Z-J Ding†

CCAST (World Laboratory), PO Box 8730, Beijing, 100080, and Fundamental Physics Centre, University of Science and Technology of China, Hefei 230026, Anhui, People's Republic of China

Received 5 September 1997, in final form 8 December 1997

Abstract. A scheme for calculating the complex self-energy of electrons moving in a real metal surface region is proposed. The approach is based on a quantum formula that uses a Drude–Lindhard model bulk dielectric function $\varepsilon(\boldsymbol{q}, \omega)$ for describing free-electron metal. The experimental energy-loss function $\mathrm{Im}\{-1/\varepsilon(\omega)\}$ is fitted to a finite sum of the modelled energy-loss functions and a corresponding expression for the complex self-energy is derived. Calculated differential inelastic scattering cross-section results are given for Mg, Ag and Au to show the surface and bulk excitation modes in these metals. The z-dependent inelastic mean free path and stopping power near a surface region are also obtained. The approach provides a practical scheme to be used in quantitative surface electron spectroscopy.

1. Introduction

A quantitative description of the energy spectra of electrons emitted from a solid surface requires a full knowledge of the electron inelastic scattering processes made up of surface excitations as well as bulk excitations of solid electrons. More specifically, one needs to know the total scattering cross-section and the differential cross-section in terms of the momentum transfer and loss energy. In the preceding paper [1], a formalism for the electron self-energy was presented for an electron penetrating through a surface from the interior of a solid to the vacuum. The inelastic cross-section depending on the distance from the surface and the velocity vector can be obtained from the imaginary part of the self-energy for any metal of known dielectric function $\varepsilon(\boldsymbol{q}, \omega)$. An expression for the self-energy using the Drude–Lindhard model dielectric function was derived for a free-electron material. Unfortunately, no exact dependence of $\varepsilon(\boldsymbol{q}, \omega)$ on momentum transfer is known either theoretically and experimentally for a variety of materials of practical interest, including noble metals and transition metals. To get the necessary information concerning the electron inelastic scattering in a real metal, one has to use the experimental values of the optical dielectric function $\varepsilon(\omega)$ and extrapolate these data from the optical limit to other momentum transfers.

To do this, Ritchie and Howie [2] have suggested a method for obtaining an approximate energy-loss function for arbitrary q-values from an optical energy-loss function. In brief, a procedure for fitting to the experimental data is carried out to obtain the parameters involved in a sum of Drude–Lindhard model energy-loss functions at $q = 0$. Further extending this to

† E-mail: zjding@nsc.ustc.edu.cn.

0953-8984/98/081753+13$19.50

finite q-values by assuming a plasmon dispersion leads to the required $\mathrm{Im}\{-1/\varepsilon(q,\omega)\}$. The spirit of this method for obtaining the q-dependent dielectric function has been employed by many authors [3–7] since then in their theories of electron inelastic scattering.

In this paper, a scheme for the calculation of the electron self-energy in the surface region of a real metal is developed by combining the above-mentioned formalism with a method using optical data (section 2). Numerical calculations of the differential energy-loss cross-section, inelastic mean free path (IMFP) and stopping power have been performed for several metals. Their dependence on the kinetic energy, the distance from a surface and the take-off angle have also been presented (section 3).

2. Theory

Let us decompose a bulk energy-loss function into N terms of the Drude–Lindhard model energy-loss function:

$$\mathrm{Im}\left\{\frac{-1}{\varepsilon(q,\omega)}\right\} = \sum_{i=1}^{N} a_i \,\mathrm{Im}\left\{\frac{-1}{\varepsilon(q,\omega;\omega_{p_i},\gamma_i)}\right\} \tag{1}$$

where the $3N$ parameters a_i, γ_i and ω_{p_i} are respectively the oscillator strength, energy and width of the ith oscillator, which are determined from an experimental optical energy-loss function using a fitting procedure:

$$\mathrm{Im}\left\{\frac{-1}{\varepsilon(\omega)}\right\} = \sum_{i=1}^{N} a_i \,\mathrm{Im}\left\{\frac{-1}{\varepsilon(0,\omega;\omega_{p_i},\gamma_i)}\right\}. \tag{2}$$

This implies that core excitations in a solid are treated as similar to free electrons, in the spirit of a statistical model [8], and described by a Drude–Lindhard dielectric function for a plasmon pole with finite damping:

$$\varepsilon_i \equiv \varepsilon(q,\omega;\omega_{p_i},\gamma_i) = 1 + \frac{\omega_{p_i}^2}{\beta^2 q^2 + q^4/4 - \omega(\omega + \mathrm{i}\gamma_i)} \tag{3}$$

while the unnecessary constant ω_{g} in equation (39) of [1] is discarded.

From the Kramers–Kronig relation

$$\mathrm{Re}\left\{\frac{1}{\varepsilon(q,\omega)} - 1\right\} = \frac{2}{\pi}\,\mathcal{P}\int_0^\infty \mathrm{Im}\left\{\frac{1}{\varepsilon(q,\omega')} - 1\right\}\frac{\omega'\,\mathrm{d}\omega'}{\omega'^2 - \omega^2} \tag{4}$$

we readily get

$$\frac{1}{\varepsilon(q,\omega)} - 1 = \sum_{i=1}^{N} a_i\left(\frac{1}{\varepsilon_i} - 1\right). \tag{5}$$

The bulk self-energy term (equation (22) of [1]) is therefore a linear combination of each bulk component with ε_i:

$$\Sigma^{\mathrm{b}}[\varepsilon] = \frac{2}{(2\pi)^2}\int\frac{\mathrm{d}\boldsymbol{q}}{q^2}\int_0^\infty \mathrm{d}\omega\left(\frac{1}{\varepsilon} - 1\right)\delta(\omega - \boldsymbol{q}\cdot\boldsymbol{v}) = \sum_{i=1}^{N} a_i\,\Sigma^{\mathrm{b}}[\varepsilon_i]. \tag{6}$$

But the surface terms are not such simple linear combinations. Using equation (5), we find for the surface dielectric function

$$\frac{1}{\varepsilon_{\mathrm{s}}(q_\parallel,\omega)} - 2 = \sum_{i=1}^{N} a_i\left\{\frac{1}{\varepsilon_{\mathrm{s}i}(q_\parallel,\omega)} - 2\right\} \tag{7}$$

Table 1. A comparison of the Ω_p-values, where Ω_p^2 equals: $4\pi ne^2/m$ (theoretical definition); $2\pi^{-1}\int_0^\infty \omega\ \mathrm{Im}\{-1/\varepsilon(\omega)\}\ \mathrm{d}\omega$ (the f-sum rule obtained from an optical energy-loss function); $\sum_{i=1}^{N} a_i\omega_{p_i}^2$ (as fitted by equation (2) and a sum rule).

	Ω_p (eV)			
	Theory	Sum rule	Fitted	N
Mg	26.7	28.7	29.1	44
Si	31.1	29.6	30.2	31
Ag	61.6	63.1	64.5	44
Au	80.1	76.3	78.4	50

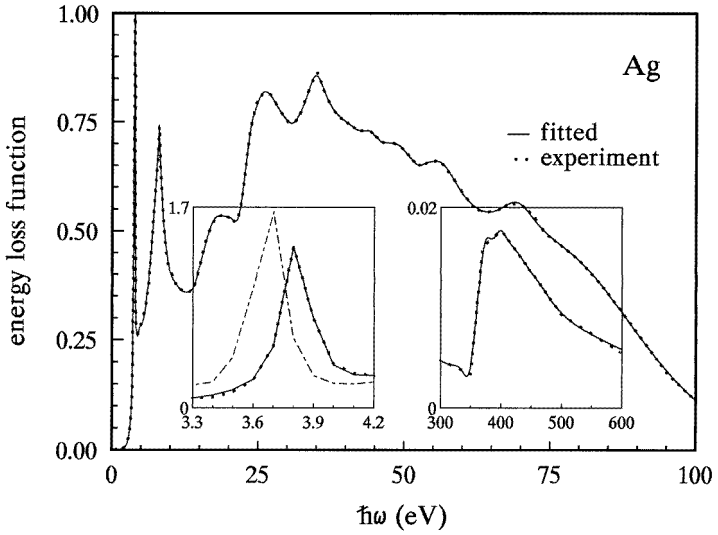

Figure 1. A comparison of the optical bulk energy-loss function $\mathrm{Im}\{-1/\varepsilon(\omega)\}$ derived by means of a fitting (solid line) to experimental data (dotted line) for silver. The chain line in the left-hand inset is the optical surface energy-loss function $\mathrm{Im}\{-1/[1+\varepsilon(\omega)]\}$.

where

$$\frac{1}{\varepsilon_{si}} = 1 + \frac{q_\parallel}{\pi}\int_{-\infty}^{\infty}\frac{\mathrm{d}q_\perp}{q^2\varepsilon_i} \tag{8}$$

and the self-energy term for $z<0$ due to the image charge (equation (23) of [1]) is

$$\begin{aligned}\Sigma^{\mathrm{i}}[\varepsilon] &= -\frac{2\mathrm{i}}{(2\pi)^3}\int \mathrm{d}\boldsymbol{q}_\parallel\int_0^\infty \mathrm{d}\omega\int_{-\infty}^{\infty}\frac{\mathrm{d}q_\perp}{q^2\varepsilon}\left(\frac{\mathrm{e}^{-2\mathrm{i}q_\perp z}}{\omega-\boldsymbol{q}\cdot\boldsymbol{v}-\mathrm{i}\eta}-\frac{\mathrm{e}^{2\mathrm{i}q_\perp z}}{\omega-\boldsymbol{q}\cdot\boldsymbol{v}+\mathrm{i}\eta}\right)\\ &= \left(1-\sum_{i=1}^{N}a_i\right)\Sigma^{\mathrm{i}}[1]+\sum_{i=1}^{N}a_i\,\Sigma^{\mathrm{i}}[\varepsilon_i]\end{aligned} \tag{9}$$

where $\Sigma^{\mathrm{i}}[1]$ is

$$\Sigma^{\mathrm{i}}[\varepsilon=1] = -\frac{\mathrm{i}}{2\pi}\int_0^\infty \mathrm{d}\omega\int_0^\infty \mathrm{d}q_\parallel\ \{P_2^-[1]-P_2^+[1]\}. \tag{10}$$

Since

$$P_n^{\pm}[1] = \frac{1}{2\pi}\int_0^{2\pi} \mathrm{d}\varphi\ \frac{q_\parallel}{\pi}\int_{-\infty}^{\infty}\frac{\mathrm{d}q_\perp}{q^2}\ \frac{\mathrm{e}^{\pm \mathrm{i}nq_\perp z}}{\omega - \boldsymbol{q}\cdot\boldsymbol{v} \pm \mathrm{i}\eta}$$
$$= \frac{1}{2\pi}\int_0^{2\pi}\frac{\mathrm{e}^{nq_\parallel z}\ \mathrm{d}\varphi}{\omega - \boldsymbol{q}_\parallel\cdot\boldsymbol{v}_\parallel \pm \mathrm{i}q_\parallel v_\perp} = \mathrm{e}^{nq_\parallel z}\ Q_0(\pm \mathrm{i}q_\parallel) \tag{11}$$

equation (10) becomes

$$\Sigma^{\mathrm{i}}[1] = -\frac{1}{\pi}\int_0^{\infty}\mathrm{d}\omega\int_0^{\infty}\mathrm{d}q_\parallel\ \mathrm{e}^{2q_\parallel z}\,\mathrm{Im}\{Q_0(\mathrm{i}q_\parallel)\}. \tag{12}$$

Similarly, on finding $H[1] = \exp(q_\parallel z)$, the self-energy term for $z < 0$ due to surface charges (equation (24) of [1]) reads

$$\Sigma^{\mathrm{s}}[\varepsilon] = \frac{\mathrm{i}}{\pi}\int_0^{\infty}\mathrm{d}\omega\int_0^{\infty}\mathrm{d}q_\parallel\ \varepsilon_{\mathrm{s}}(q_\parallel,\omega)\left\{\left(1-\sum_{i=1}^{N}a_i\right)\mathrm{e}^{q_\parallel z}+\sum_{j=1}^{N}a_i H[\varepsilon_i]\right\}$$
$$\times\ \left\{\left(1-\sum_{i=1}^{N}a_i\right)\mathrm{e}^{q_\parallel z}\left[Q_0(-\mathrm{i}q_\parallel)-Q_0(\mathrm{i}q_\parallel)\right]+\sum_{i=1}^{N}a_i\left[P_1^-[\varepsilon_i]-P_1^+[\varepsilon_i]\right]\right\}. \tag{13}$$

The self-energy terms for $z > 0$ (equations (28) and (29) of [1]) are

$$\Sigma_1[\varepsilon] = \frac{\mathrm{i}}{2\pi}\int_0^{\infty}\mathrm{d}\omega\int_0^{\infty}\mathrm{d}q_\parallel\ \mathrm{e}^{-2q_\parallel z}(1-2\varepsilon_{\mathrm{s}})\left[Q_0(-\mathrm{i}q_\parallel)-Q_0(\mathrm{i}q_\parallel)\right] \tag{14}$$

and

$$\Sigma_2[\varepsilon] = \frac{\mathrm{i}}{2\pi}\int_0^{\infty}\mathrm{d}\omega\int_0^{\infty}\mathrm{d}q_\parallel\ \mathrm{e}^{-q_\parallel z}\left\{\left[1-2\varepsilon_{\mathrm{s}}\left(1-\sum_{i=1}^{N}a_i\right)\right]\left[Q_1^-(-\mathrm{i}q_\parallel)-Q_1^+(\mathrm{i}q_\parallel)\right]\right.$$
$$\left.+\ (1-2\varepsilon_{\mathrm{s}})\left[Q_1^-(\mathrm{i}q_\parallel)-Q_1^+(-\mathrm{i}q_\parallel)\right]-2\varepsilon_{\mathrm{s}}\sum_{i=1}^{N}a_i\left[R^-[\varepsilon_i]-R^+[\varepsilon_i]\right]\right\}. \tag{15}$$

3. Results and discussion

In general, an optical energy-loss function extends over a wide photon energy range from 10^0 to 10^3 eV. The lower-energy region exhibits a complex structure due to interband transitions. Inner-shell ionization edges can be observed at high energies. For the calculation of the IMFP of keV electrons, the whole photon energy range should be considered. To ensure the accuracy of the fitting to the optical energy-loss function, a sufficiently large number of Drude–Lindhard terms is therefore necessary. It is obvious that the set of parameters is not unique. To reduce the computing work, we allow a negative value of a_i. This is an efficient way of accelerating the convergence at an inner-shell edge by adding more terms. Meanwhile, the f-sum rule can still be obeyed. Table 1 compares the Ω_p-values obtained by a fitting procedure using equation (2) with theoretical and bulk f-sum-rule values for several elements. The input optical data were taken from a handbook [9] for Au, Ag and Si, and from a compilation [10] for Mg.

A SIMPLEX optimizing routine [11], which enables a fast convergence to the required accuracy to be achieved, was used to find over a hundred parameters involved in several tens of Drude–Lindhard terms. Figure 1 shows an example of the fitting result for Ag. The insets are magnifications at a surface plasmon loss peak and an $M_{4,5}$ edge.

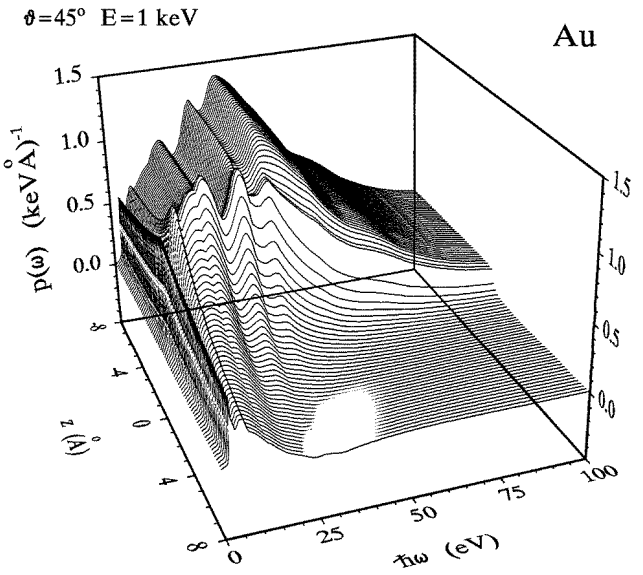

(a)

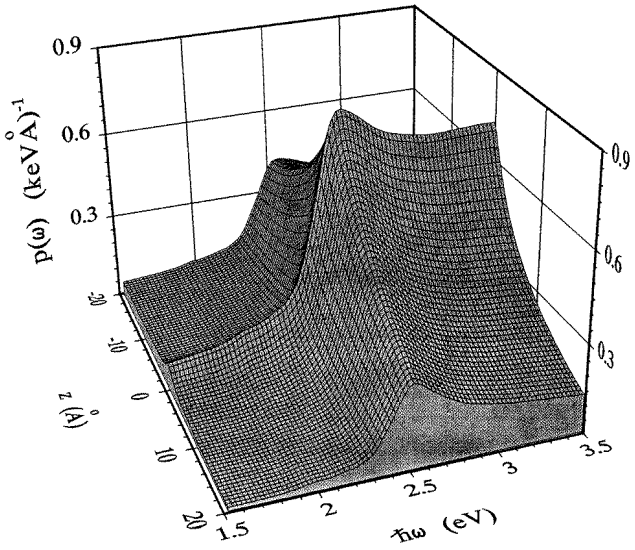

(b)

Figure 2. A perspective view of the inelastic scattering differential cross-section as a function of ω and z for Au. (a) A wide energy range including interband transitions. (b) A low-energy region showing a surface peak.

In the present work, we have chosen $\beta = \sqrt{\frac{2}{3}E_{\mathrm{F}}}$ in equation (3) so that the dispersion is that of bulk plasmon in a free-electron gas. This differs from a simpler dispersion equation used in [1]. Because the experimental investigations of the dispersion were mainly carried out to study plasmons, it is difficult to assess how accurately these dispersion relations

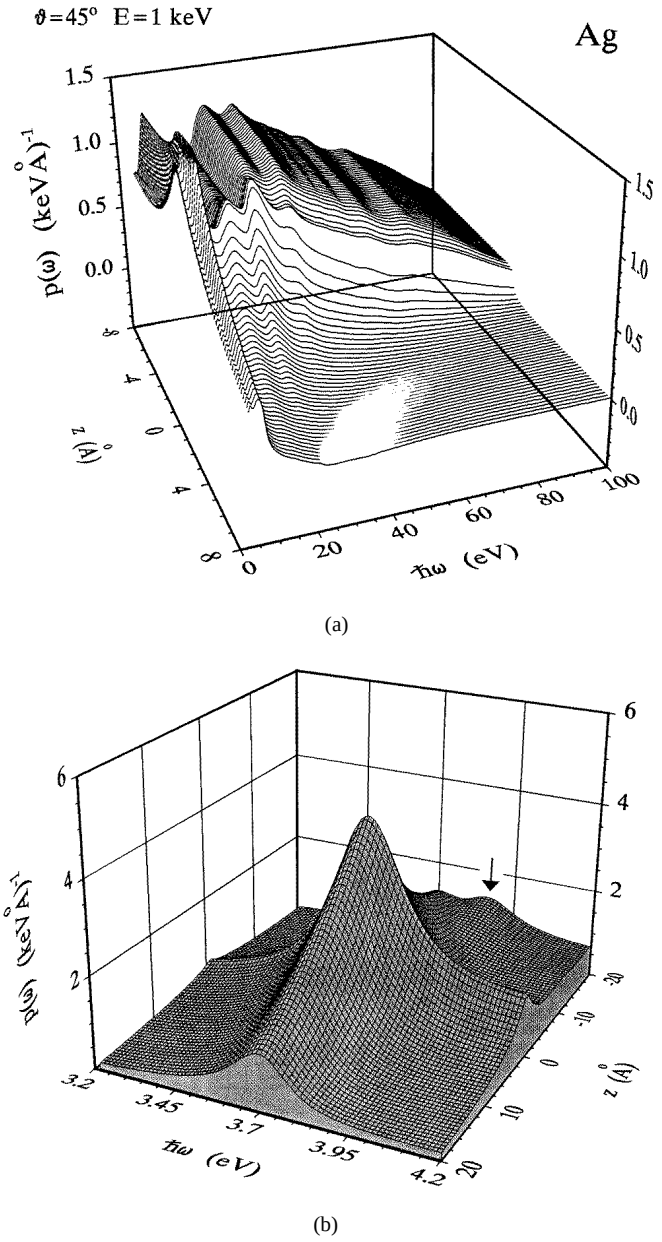

Figure 3. A perspective view of the inelastic scattering differential cross-section as a function of ω and z for Ag. (a) A wide energy range including interband transitions; the unseen region where $\omega < 4.2$ eV is magnified in (b). The arrow indicates a bulk feature.

describe interband transitions in transition and noble metals. The dispersion coefficient affects the shape of the wave-vector-dependent dielectric function and, hence, slightly affects the value of the self-energy. For bulk terms, it has been shown that the resultant differences in IMFP and stopping power caused by using different values of β are not significant [12].

Only the calculation result for the imaginary part of the self-energy will be presented

below. Figure 2 shows the varying of the inelastic scattering differential cross-section with z for Au. Roughly speaking, the overall shape of the cross-section transforms from the shape of the bulk energy-loss function $\mathrm{Im}\{-1/\varepsilon(\omega)\}$ to that of the surface energy-loss function $\mathrm{Im}\{-1/[1+\varepsilon(\omega)]\}$, as z increases to 0^-. It is clear that certain peak heights at lower energy-loss positions increase considerably as $z \to 0^-$, reach maximum values at $z = 0$ and then decrease slowly as $z \to \infty$. The peak positions slightly shift to the lower-energy side with z due to the intensity reduction on the higher-energy side. This slow damping behaviour with z in the vacuum region indicates that those peaks may reasonably be identified as dominant surface modes in a noble metal. Figure 2(b) is an enlargement around the lowest surface peak at 2.6 eV, which has been observed in a reflection electron energy-loss spectroscopy (REELS) experiment [13].

Figure 3 demonstrates a similar case for another noble metal, Ag. Note that the shoulder at 3.86 eV in figure 3(b) is a bulk feature, corresponding to the sharp peak at 3.8 eV in the bulk energy-loss function shown by figure 1. The dominant loss peak at 3.72 eV certainly has a surface loss character, corresponding to the 3.7 eV peak in the surface energy-loss function. The experimental values of these bulk and surface plasmon energies are respectively 3.78 eV and 3.63 eV [14]. Experimental REELS spectra [13] taken at beam energies of 1.5 keV and 200 eV have peaks at respectively 3.8 eV and 3.6 eV, which were assigned to combinations of the surface plasmon excitation and bulk plasmon excitation. However, the details of how each mode contributes to the observed loss peak were unknown. The present theory clearly reveals that surface plasmon excitation is the main characteristic in REELS experiments on silver. However, a quantitative analysis should be done with a Monte Carlo simulation because the loss peak intensity depends considerably on the experiment conditions.

Figures 4 and 5 show the case of two further free-electron-like materials, Si and Mg. They have plasmon loss peaks at lower loss energies. But we will mainly note the inner-shell edge in figures 4(b) and 5(b). The $L_{2,3}$ edge varies almost constantly with z from the interior of the solid to the surface. When z increases from the surface it quickly drops down. This is quite reasonable because a scattering electron far from the surface can hardly interact with core electrons in an atom.

We can compare the present result with our previous calculation [15]. With a δ-function-type modelling energy-loss function, the surface terms become oscillating in z and ω in the moderate-z region and can hardly approach zero as $z \to -\infty$. This is probably due to a convergence problem in the limit of an infinitely small damping constant. The present calculation overcomes this shortcoming as well as significantly reducing the computation time: a summation over finite terms replaces an integration that requires a fine grid spacing for numerical calculation.

Figure 6 shows the kinetic energy dependence of the differential cross-section. For $z < 0$ and in the surface region, by comparing figure 6(a) with figure 6(b), we can see that the surface effect increases the energy-loss probability and stopping power mainly at low E- and ω-values. For $z > 0$, there is the same tendency. However, $p(\omega)$ becomes physically meaningless—negative, when $\omega/E \to 1$ with decreasing E. Obviously, this is due to the fast-electron approximation made in the theory [1]. These negative values must be abandoned in the calculation of the IMFP, $\lambda = (\mathrm{Im}\,\bar{\Sigma})^{-1}$, and the electron stopping power. Note that the scaled self-energy is defined by equation (64) of [1].

The z-dependence of the IMFP is shown in figure 7. At lower energies, the total scattering probability increases near the surface region, while at high energies, the surface effect is very small for an electron before it leaves the surface. The damping of the inverse IMFP with z in the vacuum region seems to be heavier than that predicted by a semi-classical theory [16]. Note that, in order to retain the same extent of approximation for the

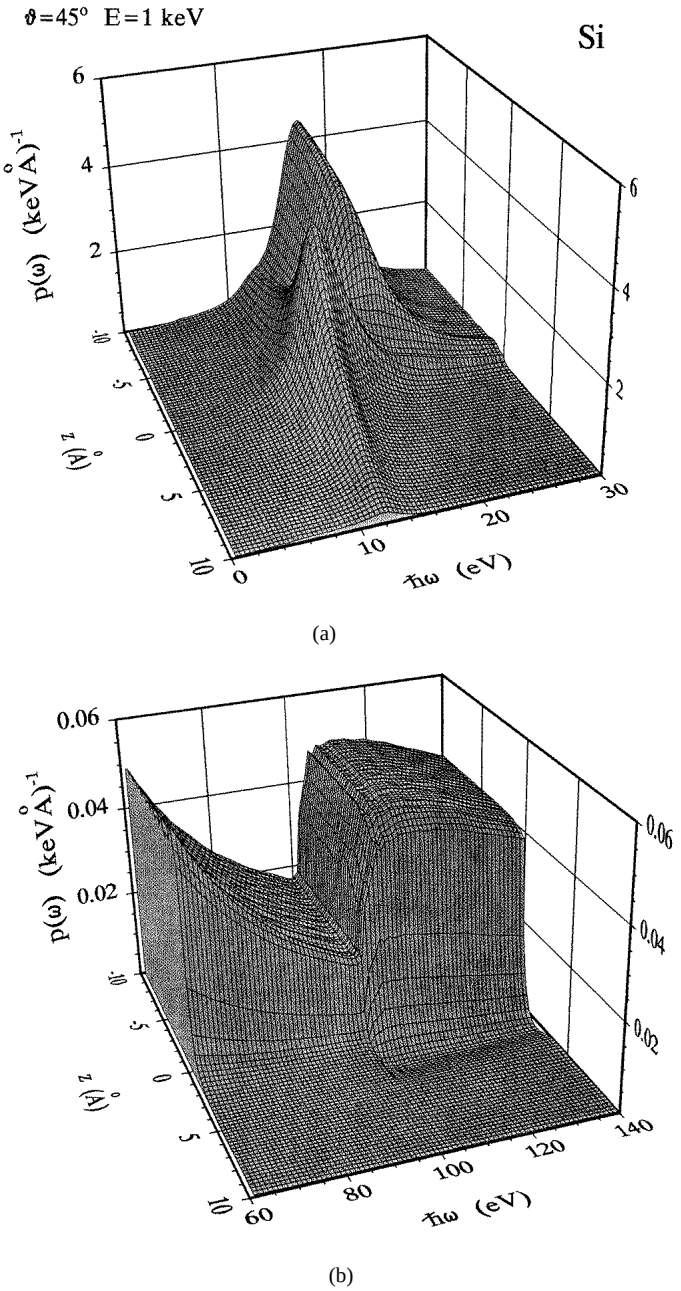

Figure 4. A perspective view of the inelastic scattering differential cross-section as a function of ω and z for Si. (a) The plasmon energy-loss region. (b) The $L_{2,3}$-edge region.

bulk term as for the surface terms, we have used $\delta(\omega - \boldsymbol{q}\cdot\boldsymbol{v})$ in equation (6) instead of $\delta(\omega - \boldsymbol{q}\cdot\boldsymbol{v} + \frac{1}{2}q^2)$. Therefore, the integration limits of q are taken as $q_+ = \infty$ and $q_- = \omega/v$ in equation (61) of [1] instead of $q_\pm = \sqrt{2E} \pm \sqrt{2(E-\omega)}$. This leads to a smaller bulk IMFP compared with that obtained by calculation by Tanuma *et al* [17].

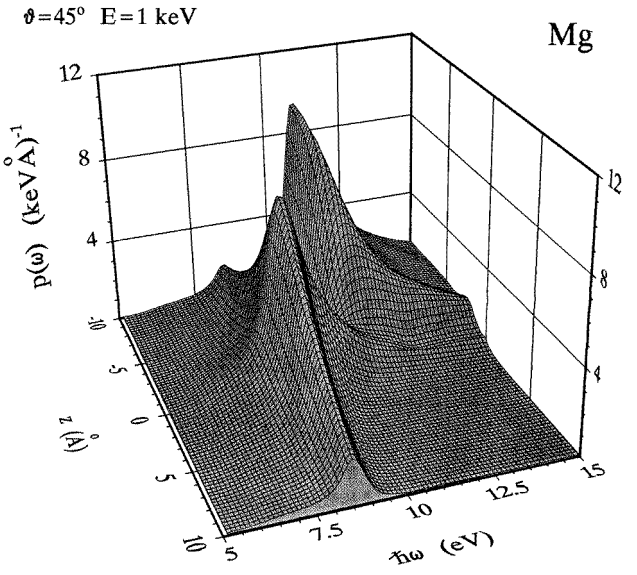

(a)

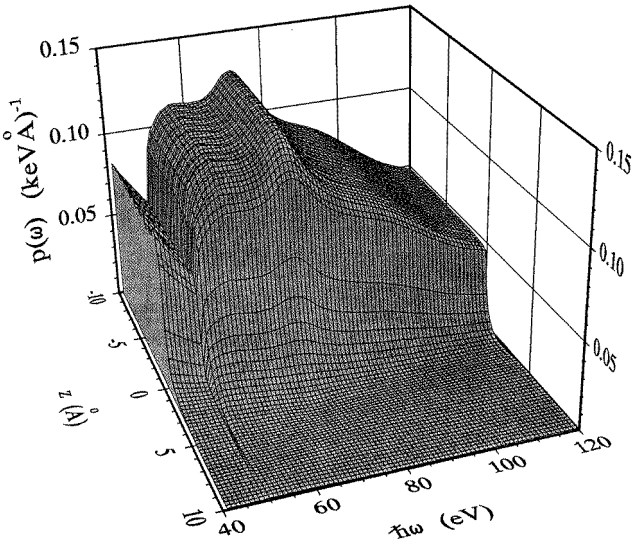

(b)

Figure 5. A perspective view of the inelastic scattering differential cross-section as a function of ω and z for Mg. (a) The plasmon energy-loss region. (b) The $L_{2,3}$-edge region.

Figure 8 illustrates the energy dependency of the space-varying inverse IMFP and stopping power:

$$-\mathrm{d}E/\mathrm{d}x = \int_0^{E-E_\mathrm{F}} \omega \,\mathrm{Im}\,\bar{\Sigma}(z|\omega)\;\mathrm{d}\omega. \tag{16}$$

Each of these has shown a maximum at around a hundred electron volts. The stopping power

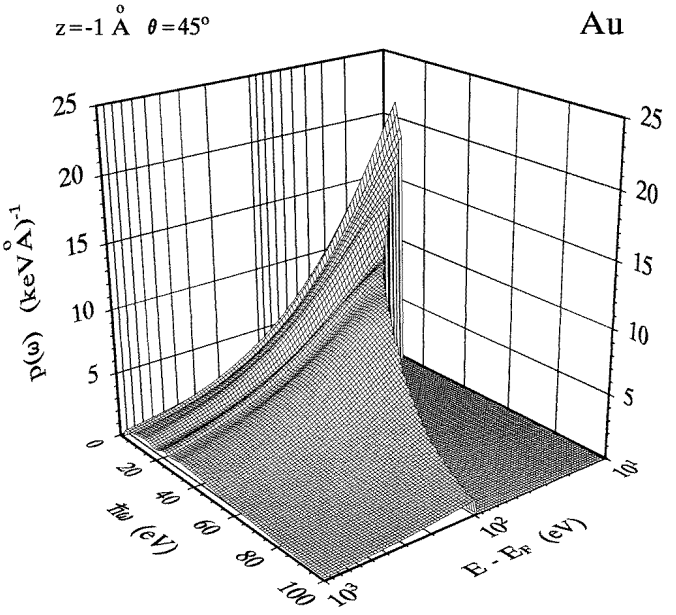

(a)

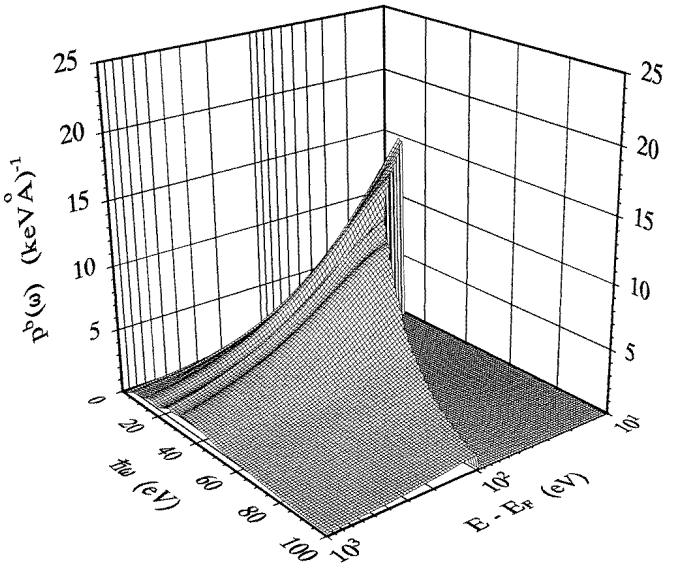

(b)

Figure 6. A perspective view of the inelastic scattering differential cross-section as a function of ω and E for Au. A cut-off is made at $\omega = E - E_F$. (a) The total $p(\omega)$ for $z < 0$. (b) The bulk term $p^b(\omega)$. (c) The total $p(\omega)$ for $z > 0$.

has almost no maximum in the surface region, which is not true for the inverse IMFP. This is because, although the scattering probability increases at the surface, the energy-loss value is decreased by the surface modes. Figure 9 presents the angular dependence of the IMFP.

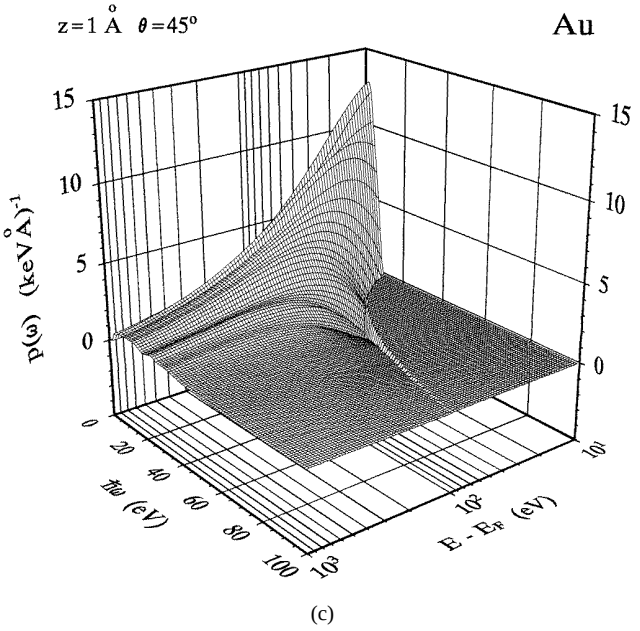

(c)

Figure 6. (Continued)

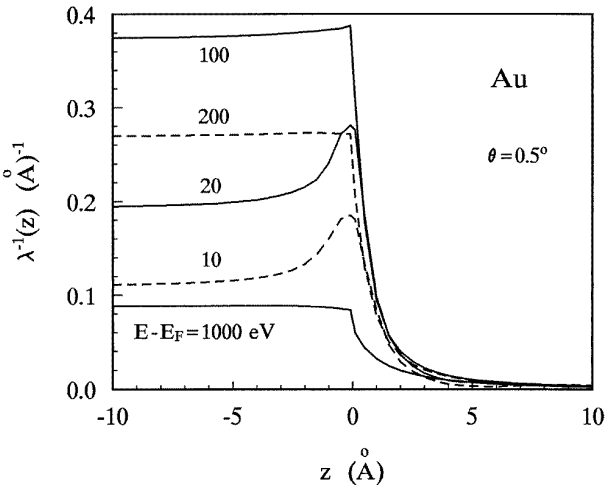

Figure 7. The z-dependency of the inverse inelastic mean free path.

The inverse IMFP increases smoothly with the take-off angle θ for $z < 0$ and the opposite tendency is found for $z > 0$.

4. Conclusions

In conclusion, we have derived an expression for the self-energy of an electron interacting with a real metal surface. The formulation is based on fitting an experimental energy-

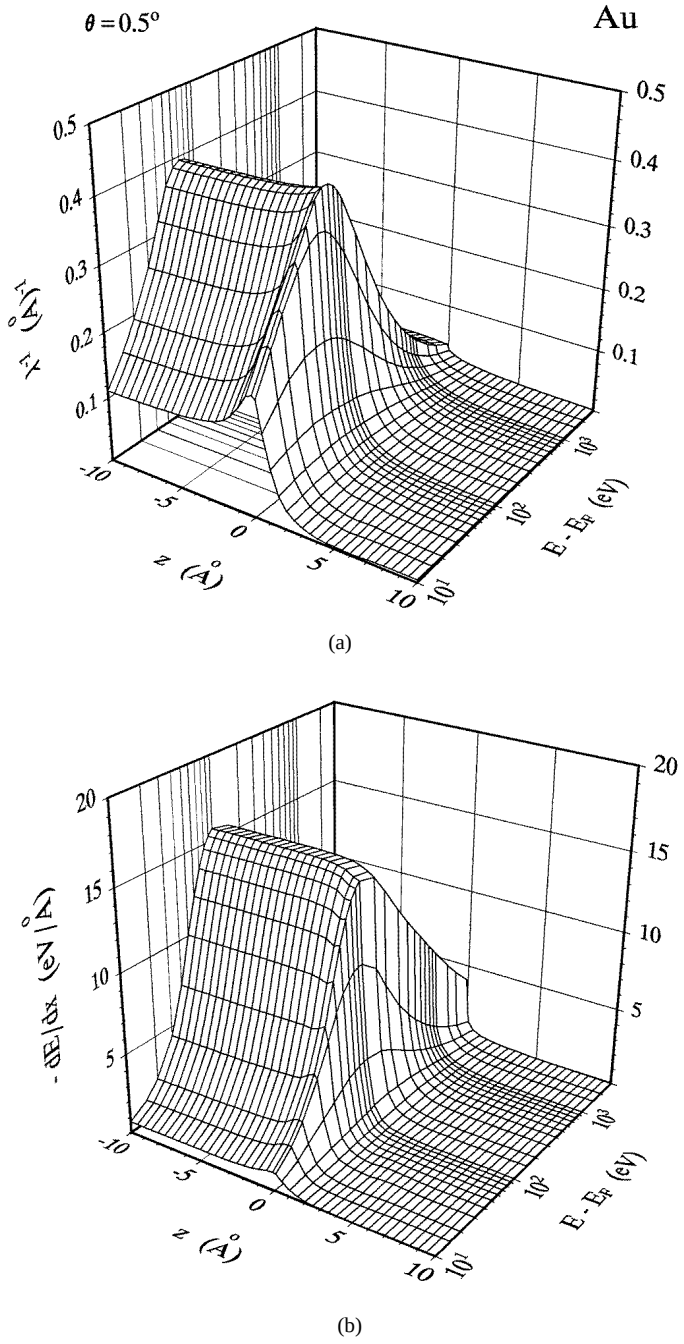

(a)

(b)

Figure 8. A perspective view of (a) the inverse inelastic mean free path and (b) the stopping power as functions of z and E.

loss function $\mathrm{Im}\{-1/\varepsilon(\omega)\}$ with a sum of Drude–Lindhard model energy-loss functions. Numerical calculations have been performed for several metals. Surface excitation modes in these metals can be understood on the basis of a space-varying differential energy-loss

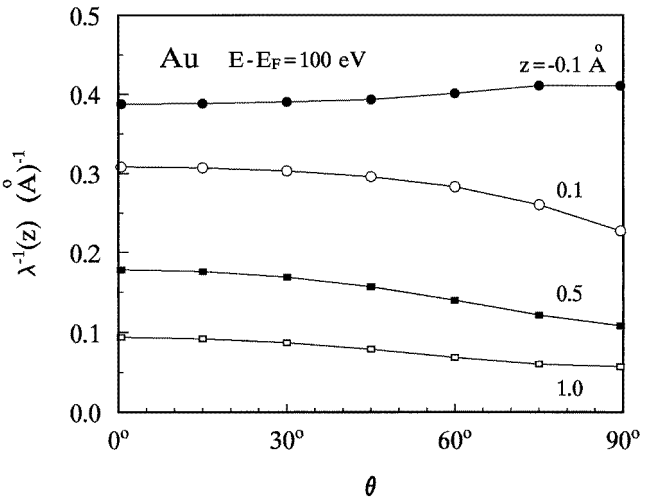

Figure 9. The dependence on the take-off angle of the inverse inelastic mean free path.

cross-section. The result of the calculation is reasonable at high energies where the Born approximation is valid.

Acknowledgments

This work was supported in part by the National Natural Science Foundation of China, the Foundation for High Performance Computing, and the Chinese Academy of Science through the grants CAS Presidential Foundation and *Liu Xue Hui Guo Ren Yuan Ze You Zi Zhu*. Some of the data presented here were calculated using a parallel computer, Dawn-1000, at the High Performance Computing Centre at Hefei.

References

[1] Ding Z J 1998 *J. Phys.: Condens. Matter* **10** 1733
[2] Ritchie R H and Howie A 1977 *Phil. Mag.* A **36** 463
[3] Tougaard S 1987 *Solid State Commun.* **61** 547
[4] Yubero F and Tougaard S 1992 *Phys. Rev.* B **46** 2486
[5] Tung C J, Chen Y F, Kwei C M and Chou T L 1994 *Phys. Rev.* B **49** 16 684
[6] Yubero F, Sanz J M, Ramskov B and Tougaard S 1996 *Phys. Rev.* B **53** 9719
[7] Akkerman A, Boutboul T, Breskin A, Chechik R, Gibrekhterman A and Lifshitz Y 1996 *Phys. Status Solidi* b **198** 769
[8] Tung C J, Ashley J C and Ritchie R H 1979 *Surf. Sci.* **81** 427
[9] Palik E D (ed) 1985 *Handbook of Optical Constants of Solids* (Orlando, FL: Academic)
[10] Hagemann H-J, Gudat W and Kunz C 1974 *Deutsches Elektronen-Synchrotron (DESY) Report* SR-74/7
[11] Nelder J A and Mead R 1965 *Comput. J.* **8** 308
[12] Ding Z J and Shimizu R 1996 *Scanning* **18** 92
[13] Ingram J C, Nebesny K W and Pemberton J E 1990 *Appl. Surf. Sci.* **44** 293
[14] Raether H 1980 *Excitation of Plasmons and Interband Transitions by Electrons* (Berlin: Springer) p 139
[15] Ding Z J 1997 *Phys. Rev.* B **55** 9999
[16] Chen Y F and Kwei C M 1996 *Surf. Sci.* B **364** 131
[17] Tanuma S, Powell C J and Penn D R 1991 *Surf. Interface Anal.* **17** 911